JOINT INSTITUTE FOR AERONAUTICS AND ACOUSTICS

NASA-CR-201844

National Aeronautics and
Space Administration
Ames Research Center

JIAA TR 113

Stanford University

ROLL-YAW CONTROL AT HIGH ANGLE OF ATTACK BY FOREBODY TANGENTIAL BLOWING

N. Pedreiro, S. M. Rock, Z. Z. Celik and L. Roberts

Department of Aeronautics and Astronautics
Stanford University
Stanford, CA 94305

October 1995

Abstract

The feasibility of using forebody tangential blowing to control the roll-yaw motion of a wind tunnel model is experimentally demonstrated. An unsteady model of the aerodynamics is developed based on the fundamental physics of the flow. Data from dynamic experiments is used to validate the aerodynamic model. A unique apparatus is designed and built that allows the wind tunnel model two degrees of freedom, roll and yaw. Dynamic experiments conducted at 45 degrees angle of attack reveal the system to be unstable. The natural motion is divergent. The aerodynamic model is incorporated into the equations of motion of the system and used for the design of closed loop control laws that make the system stable. These laws are proven through dynamic experiments in the wind tunnel using blowing as the only actuator. It is shown that asymmetric blowing is a highly non-linear effector that can be linearized by superimposing symmetric blowing. The effects of forebody tangential blowing and roll and yaw angles on the flow structure are determined through flow visualization experiments. The transient response of roll and yaw moments to a step input blowing are determined. Differences on the roll and yaw moment dependence on blowing are explained based on the physics of the phenomena.

Contents

List of Symbols

b	wing span
C_l	rolling moment coefficient, $M_x/q_\infty S_{ref} b$
C_n	yaw moment coefficient, $M_z/q_\infty S_{ref} b$
C_μ	jet momentum coefficient, $\dot{m}_j V_j / q_\infty S_{ref}$
D	diameter of fuselage
I_A, I_{arm}	inertia of the suspension system
I_M	model moments of inertia in body frame
I_{model}	inertia of the model about γ-axis
L	axial distance from tip of the forebody
$\dot{m}_j$	jet mass flow rate
M_l , M_x	rolling moment
M_z	yaw moment
M_2	moment about γ-axis
P	intersection of ϕ-axis and γ-axis
p, q, r	roll, pitch and yaw rates respectively
q_∞	dynamic pressure, $\rho U^2/2$
S_{ref}	reference area, wing planform area
U	freestream velocity
xyz	body reference frame, centered at P
ϕ	first degree of freedom, roll
γ	second degree of freedom
ρ	air density

List of Figures

Introduction

Advantages of flight at high angles of attack include increased maneuverability and increased lift during take-off and landing. At these flight conditions the aerodynamics of the vehicle are dominated by separated flow, vortex shedding and possibly vortex breakdown. These phenomena severely compromise the effectiveness of conventional control surfaces. Alternate means to control the vehicle at these flight regimes are therefore necessary. Several methods of active flow control have been proposed to provide this increased control[1-8].

The present work investigates the augmentation of aircraft flight control system by the injection of a thin sheet of air tangentially to the forebody of the vehicle. This method, known as Forebody Tangential Blowing (FTB), is proposed as an effective means of increasing the controllability of aircraft at high angles of attack[5-7]. The idea is based on the fact that a small amount of air is sufficient to change the separation line on the forebody. As a consequence the strength and position of the vortices are altered causing a change on the aerodynamic loads. Celik[5] has shown that using this method side force, roll and yaw moments can be generated for angles of attack from 20 to 50 degrees.

Experimental investigation is conducted to demonstrate the feasibility of using FTB to control the roll-yaw motion of a wind tunnel model. The model consists of a delta wing-body combination equipped with forebody slots through which blowing is applied. Experiments are conducted at a nominal incidence angle of 45 degrees

A unique apparatus that allows the model two degrees of freedom, roll and yaw, is designed and built. The apparatus is used in dynamic experiments which show that the system is unstable, its natural motion divergent. External effects of the model support system are actively canceled.

Flow visualization results revealed the vortical structure of the flow to be asymmetric even for the model at zero roll and yaw angles. The effects of blowing, roll and yaw angles on the flow structure are determined. Transient response of roll and yaw moments to step input blowing are characterized in terms of time constants. Differences on the roll and yaw moment behavior due to blowing are explained based on the physical mechanisms through which these loads are generated.

A model for the unsteady aerodynamic loads is formulated based on the basic physics of the flow. Parameters of the aerodynamic model are obtained from static and dynamic experiments. The aerodynamic model completes the equations of motion of the system which are used for the design of control laws using blowing as the only actuator. The closed loop control system is stable as is experimentally demonstrated in the wind tunnel.

Experimental Apparatus

Wind Tunnel and Model:

The wind tunnel facilities of the Aeronautics and Astronautics Department at Stanford University are used for the experiments. It consists of a closed circuit low speed wind tunnel with 0.45m x 0.45m test section. The maximum test section velocity is 50 m/s.

As illustrated in Figure 1, the model consists of a sharp leading edge delta wing with a 70 degree sweep angle and a cone-cylinder fuselage. Slots through which blowing is applied are present on both sides of the conical forebody. Air is provided to the forebody plena through flexible tubing that enters the model through the rear end of the fuselage. Tests are conducted at 20m/s and a nominal incidence angle of 45 degrees. The Reynolds number based on the wing root chord is 260,000. Tunnel blockage at the nominal configuration is 7%. Figure 2 shows a side view of the test section with the model and the supporting mechanism.

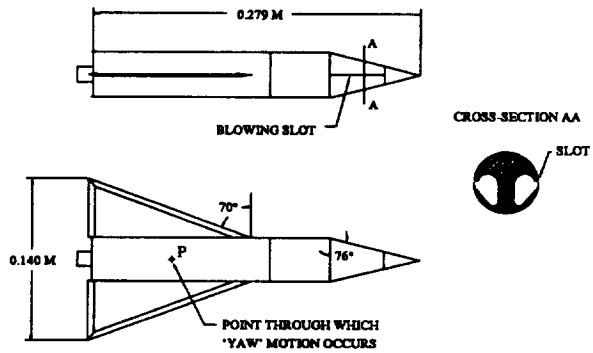

Figure 1: Wind Tunnel Model and Detail of Blowing Slots

Model Support System:

A unique support system is designed and built to implement two degrees of freedom in the model[10]. The objective is to approximate the lateral-directional dynamics of an aircraft. Of particular interest is the roll-yaw coupling at high angle of attack. The apparatus can be divided into two subsystems: The first one implements the roll degree of freedom, ϕ, and consists of a shaft mounted on bearings. The wind tunnel model is attached to the roll shaft allowing the model to rotate about its longitudinal axis. The roll subsystem is mounted on a mechanical arm that can rotate about an axis perpendicular to the models longitudinal axis (Figure 2). The mechanical arm implements the second degree of freedom, γ, and is called the 'yaw' subsystem. For small roll angles, $\dot{\gamma}$ equals the yaw rate. This approximation can be represented by relating ϕ and $\dot{\gamma}$ to the roll, pitch and yaw rates, p, q and r respectively.

$$p = \dot{\phi} \qquad q = \dot{\gamma}\sin\phi \qquad r = \dot{\gamma}\cos\phi \tag{1}$$

Mechanical constraints limit the degrees of freedom as follows: $|\phi| < 105°$ and $|\gamma| < 30°$.

An important aspect in the design of the experimental apparatus is that the dynamic properties of the support system should not dominate the dynamic response of the model. Experiments indicated that the friction in the bearings and the effect of the pressurized tubing are small when compared with the aerodynamic loads acting on the model[6].

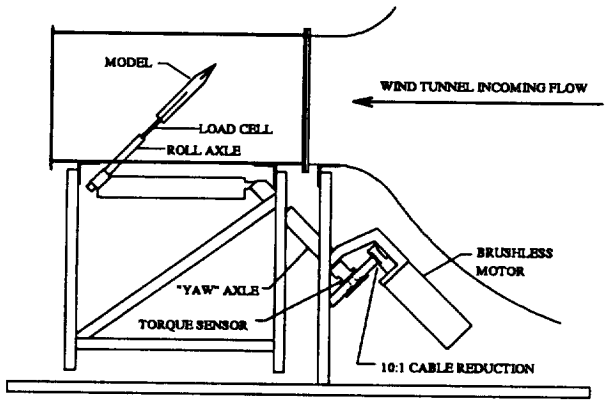

Figure 2: Side View of Test Section and Two Degrees of Freedom Model Support System

Simulations and preliminary tests indicate that the inertia of the apparatus and the gravity restoring moment have a large effect on the overall system dynamics. Therefore an electro-mechanical system to cancel these effects has been designed and implemented[10]. The concept of active cancellation consists of providing a means to apply a torque that cancels the undesired external effects. For the current system a brushless motor is used to provide a torque which is computed based on measurements of the angle γ and its angular acceleration. The same idea can be expressed in terms of the dynamic equations of the system: For the model wing at level, $\phi=0$, the equation of motion for the system can be written as:

$$(I_{arm} + I_{model})\ddot{\gamma} = M_{aerodynamic} + M_{friction} + M_{tubing} + M_{gravity} + M_{motor} \quad (2)$$

Where M represents the moment about the γ-axis.

For an ideal system:

$$I_{model}\ddot{\gamma} = M_{aerodynamic} \quad (3)$$

Therefore the torque that needs to be applied by the motor, M_{motor}, is given by:

$$M_{motor} = I_{arm}\ddot{\gamma} - M_{friction} - M_{tubing} - M_{gravity} \cong I_{arm}\ddot{\gamma} - M_{gravity} \quad (4)$$

The approximation is justified by the fact that for the current system, the inertia and gravity terms are dominant[10].

The inertia of the support, I_{arm}, is known, therefore by measuring the angular acceleration, the first term on the right hand side of the previous equation is obtained. The moment due to gravity is given by:

$$M_{gravity} = -k_G \sin\gamma \quad (5)$$

The constant k_o is a known quantity given by the product of the mass of the support by the distance of its center of gravity to the γ-axis. The angle γ is measured directly. In this way the torque that the motor should apply at any moment can be computed from these measurements.

Figure 3 shows, in block diagram form, the implementation of the active cancellation loop. A torque sensor is designed and built to satisfy the specific requirements of this application. This sensor measures the torque that the motor applies to the system. A closed loop torque control logic is designed and implemented to provide fast torque command capability necessary for the cancellation of external effects. Two high precision linear accelerometers are used to provide measurement of the angular acceleration and a low friction precision potentiometer provides the measurement for the angle γ. These two signals are fed into a computer that calculates the necessary torque command and sends it to the inner torque control loop that drives the motor.

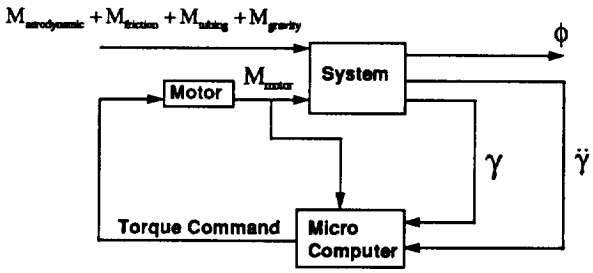

Figure 3: Block Diagram of Active Cancellation Loop.

Air Injection System:

Air can be injected independently through the slots located on both sides of the conical portion of the forebody. The amount of injected air is quantified by the jet momentum coefficient, which is defined as:

$$C_\mu \equiv \frac{\dot{m}_j V_j}{q_\infty S_{ref}} \tag{6}$$

Specially designed flowmeters are used to measure the mass flow rate from which C_μ is calculated. Servo valves are used to vary the amount of injected air. The signal from the

flowmeters is read into a computer that implements a closed loop logic for C_μ control by commanding the servo valves.

Instrumentation and Data Acquisition:

The two degrees of freedom, ϕ and γ are measured by low-friction precision potentiometers. A six-component force-torque sensor connects the model to the roll shaft and is used to provide both static and dynamic measurements of the aerodynamic loads. Flowmeters measure the amount of blowing through each plenum. Two linear accelerometers are mounted to the γ-axle. Their signals are combined to measure angular acceleration. A torque sensor connects the brushless motor to the γ-axle and therefore provides a measurement of the torque that the motor applies to the system.

For the flow visualization experiments, an argon-ion laser and an optical system are used to generate a laser sheet that is perpendicular to the model longitudinal axis. The optics is mounted on traversing system located on top of the test section allowing the laser sheet to be moved over the full length of the model. This capability is used in performing axial scans starting from the forebody and moving downstream to characterize the development of the flow structure. A smoke generator located upstream of the model is used to seed the flow. A video camera is located outside the test section aligned with the model longitudinal axis. The camera is used to record the results of the flow visualization and also the motion of the model during dynamic experiments.

Three micro computers equipped with data acquisition boards are used in the experiments. One computer is dedicated to the active cancellation loop. A second computer is used to implement the closed loop control of the vehicle, i.e. to control the amount of air injected in each plenum. A third computer is used for data acquisition.

Experimental Results

Flow Visualization:

These experiments reveal the basic structure of the flow. Although four main vortices are expected, two from the forebody and two from the wing leading edges, experiments demonstrate that in general only three separate vortical structures can be clearly identified even for a symmetric condition in which $\phi=\gamma=0$ and no blowing is applied (Figure 4b).

By performing axial scans with the laser sheet it is observed that the asymmetry starts early on the forebody, i.e. close to the tip of the cone, and scales up over the entire forebody[10]. As a result of the asymmetry one vortex will be close to the fuselage and the other will be displaced and further away as shown in Figure 4a. For the sections where the wing is present, it is observed that a vortex is formed close to the wing on the same side where the forebody vortex is far from the fuselage. For the side where the forebody vortex is close to the fuselage no wing vortex is clearly identified. A possible explanation is given for these observations: Because the forebody vortex is away from the fuselage and consequently away from the wing the wing vortex develops without much influence from the fuselage vortex. For the opposite side where the fuselage vortex is very close to the forebody the wing vortex basically merges with the forebody vortex and therefore a distinct wing vortex is not observed.

(4a) Station 1 - Forebody - L/D=3

(4b) Station 2 - Wing-Body - L/D=5

Figure 4: Smoke Flow Visualization Results - $\phi=\gamma=0$, no blowing is applied.

The effect of asymmetric blowing, i.e. blowing applied from one side only, is mainly to increase the asymmetry or invert it depending on which side the blowing is applied. Blowing moves the separation line on the forebody and can cause a change in the amount of vorticity that is shed. As a consequence the strength and positions of the vortices are affected by blowing. Experiments have shown that there is a finite amount of blowing that needs to be applied to invert the asymmetry of the flow, for the current model configuration at $\phi=\gamma=0$ this value is $C_\mu \cong 0.0045$.

The application of symmetric blowing has the effect of changing the flow structure to a more symmetric one (Figure 5). For high values of symmetric blowing the flow can be considered attached on the forebody and its structure is very symmetric even on stations where the wing is present.

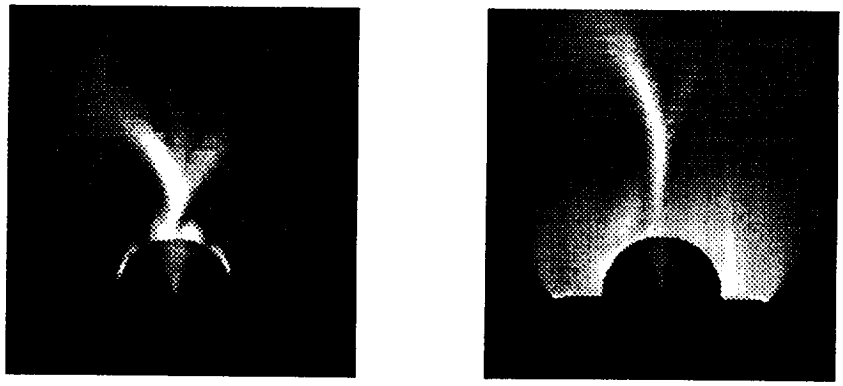

(5a) Station 1 - Forebody - L/D=3 (5b) Station 2 - Wing-Body - L/D=5

Figure 5: Smoke Flow Visualization Results - Symmetric Blowing, $\phi=\gamma=0$, $C_\mu=.0075$

Experiments show that the asymmetric structure can change significantly by a change in the roll angle. The flow structure is not as sensitive to a change in γ.

Static Aerodynamic Loads:

Static measurements for the roll and yaw moment as a function of ϕ, γ and C_μ are presented in Figures 6 through 8. A convention is adopted that right side, i.e. starboard blowing is positive and left side, i.e. port side blowing negative. In Figure 6 the effect of the roll angle on C_l and C_n is shown for $\gamma=0$ and various C_μ. The C_l curve for $C_\mu=0$ presents a change in slope for $\phi\cong-15°$.

For C_μ=.02 a change occurs at $\phi \cong -5°$. Also for C_μ=0 the C_n curve presents a large change in slope for $\phi < -15°$. The fact that these changes are not symmetric, i.e. they only occur for $\phi < 0$, indicates that they are caused by geometrical imperfections on the tip of the conical forebody.

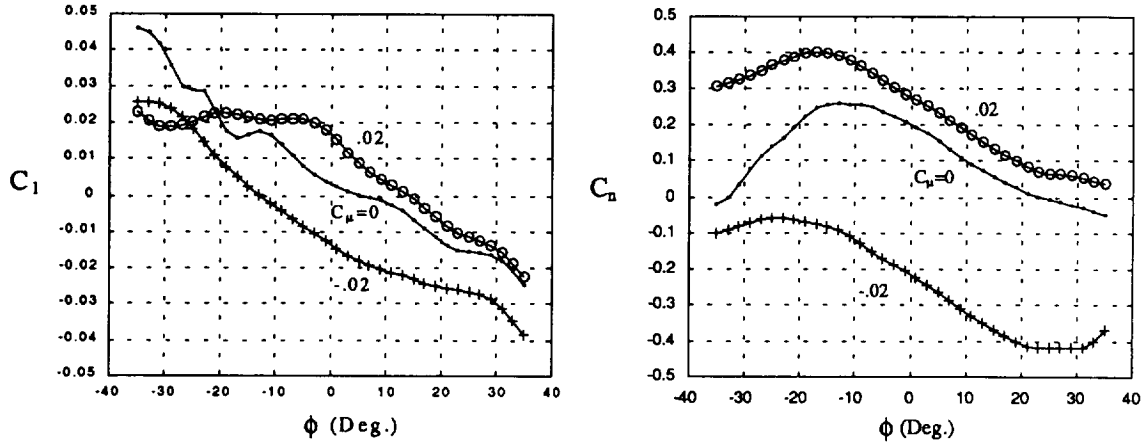

Figure 6: Roll Angle Effect on Roll and Yaw Moment Coefficients, C_l and C_n, for γ=0.

Figure 7 presents curves for C_l and C_n versus γ for ϕ=0 and various C_μ. Comparing Figures 6 and 7 shows that the slopes of the roll and yaw moment curves are not as sensitive to γ as they are to ϕ. This is in agreement with the flow visualization experiments which indicate the flow structure to be less dependent on γ than on ϕ.

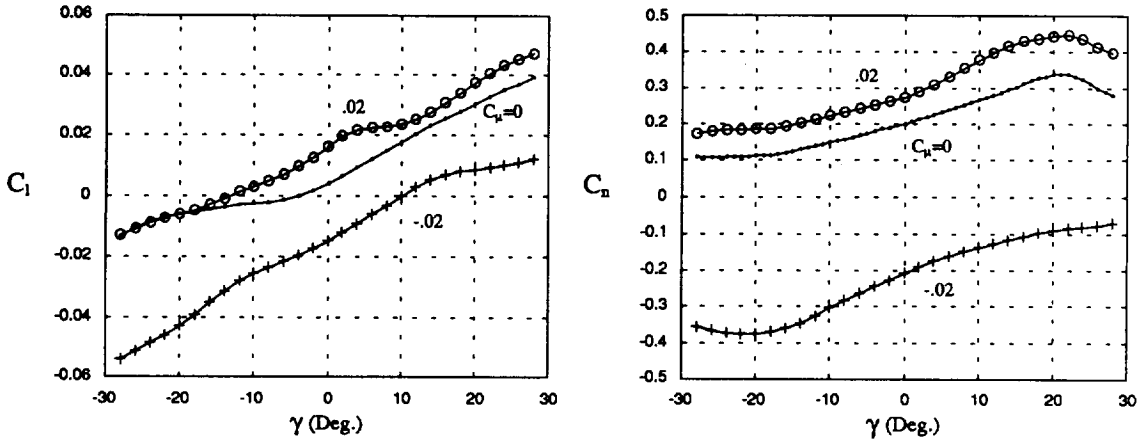

Figure 7: Effect of γ Angle on Roll and Yaw Moment Coefficients, C_l and C_n, for ϕ=0.

The effect of asymmetric blowing on C_l and C_n is shown in Figure 8 for γ=0 and various ϕ. In this case blowing is applied either on the right or left side. As seen the roll moment varies

abruptly for $|C_\mu|<0.01$ and the yaw moment presents a large variation for $0.01<C_\mu<0$. Degani[9] has shown that small amount of blowing has an effect similar to the geometric imperfections near the tip of the forebody and can cause flow instabilities that lead to asymmetry in the flow. This is the most plausible explanation for the roll moment behavior shown in Figure 8. For $|C_\mu|<0.01$ the roll moment is more sensitive to changes in C_μ than the yaw moment. This fact can be explained by the different physical mechanisms through which each of these loads are generated. For $|C_\mu|<0.01$ the contributions of the direct jet momentum to C_l and C_n are negligible. In this case, it can be considered that the roll moment is only generated at stations where the wings are present. Because the fuselage is of circular cross-section. Therefore the roll moment is determined by the flow over the wings which might be subject to large instabilities as vortex breakdown. The yaw moment is determined by the pressure distribution over the fuselage. The wings do not contribute to C_n because they are thin and only offer area perpendicular to the yaw axis. The flow over the forebody has a greater effect on the yaw moment due to its distance to the center of mass of the model. For stations on the forebody it is expected that flow instabilities are not fully grown and are therefore less important for the yaw moment.

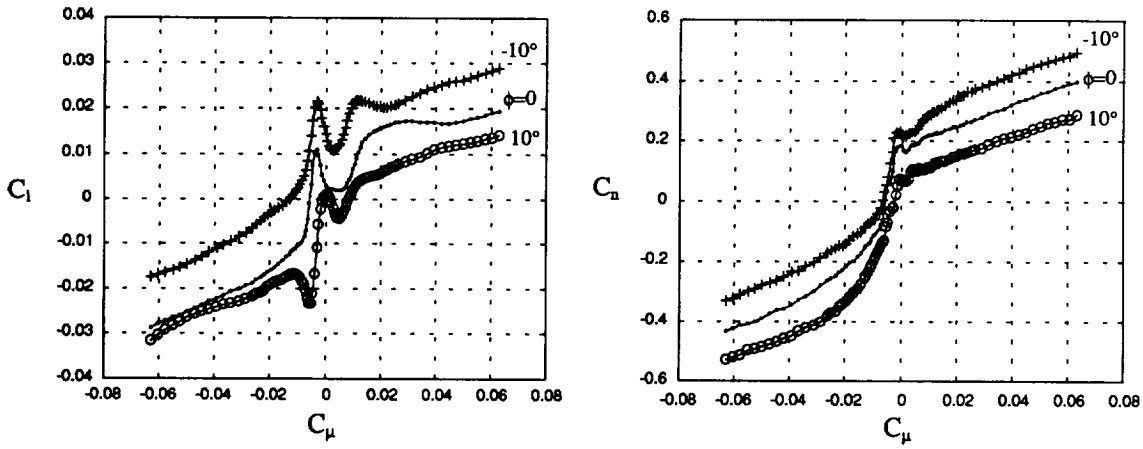

Figure 8: Effect of Asymmetric Blowing on Roll and Yaw Moment Coefficients, C_l and C_n, for $\gamma=0$.

Figure 9 shows the result of applying symmetric and incremental asymmetric blowing on the roll and yaw moment coefficients. An equal amount of blowing, $C_{\mu_{SYM}}$, is applied on both sides and additional asymmetric blowing, ΔC_μ, is applied either to the right or the left side. As seen the major effect consists in producing a linear characteristic and eliminating the sudden variations

that occur in the asymmetric blowing case. The symmetry observed in these plots agrees with the symmetric flow structure obtained from the flow visualization experiments (Figure 5).

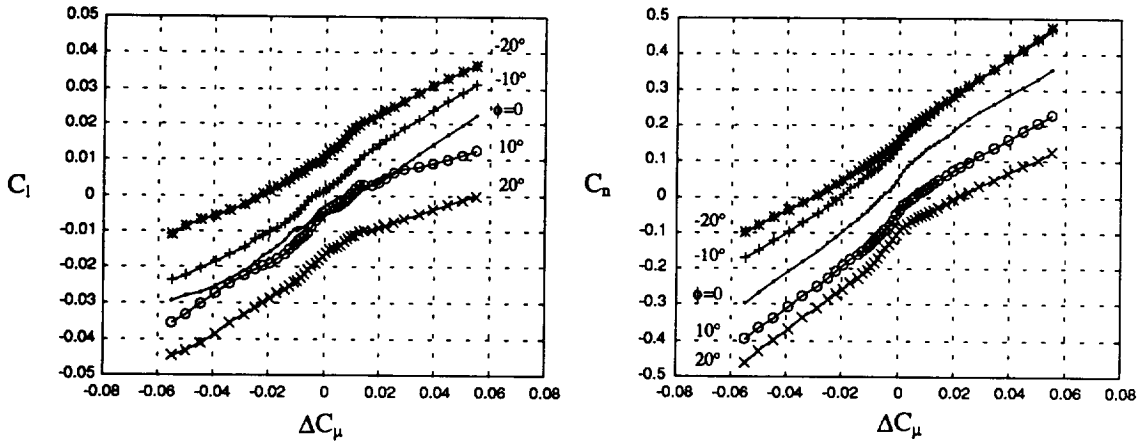

Figure 9: Effect of Symmetric Plus Asymmetric Blowing on Roll and Yaw Moment Coefficients for $C_{\mu_{SYM}}$=0.01 and γ=0.

Dynamic Experiments:

The results for the static roll and yaw moment show that these moments are not zero for $\phi=\gamma=0$ and $C_\mu=0$. Also the positive slope of the curve C_n versus γ indicates that the system is statically unstable at this condition. An experiment is performed to determine the dynamic characteristics of the system since those cannot be inferred from the static data alone: With no blowing applied the model is released from a certain initial condition. This represents the natural motion of the system and will ultimately determine if the system is stable or unstable. Figure 10 shows the time histories for ϕ and γ when the model is released from $\phi\cong\gamma\cong0$, also shown are the results from simulations using the aerodynamic model described in the following section. As seen, the system is unstable. The motion is divergent and is stopped when the system approaches the mechanical limit of γ.

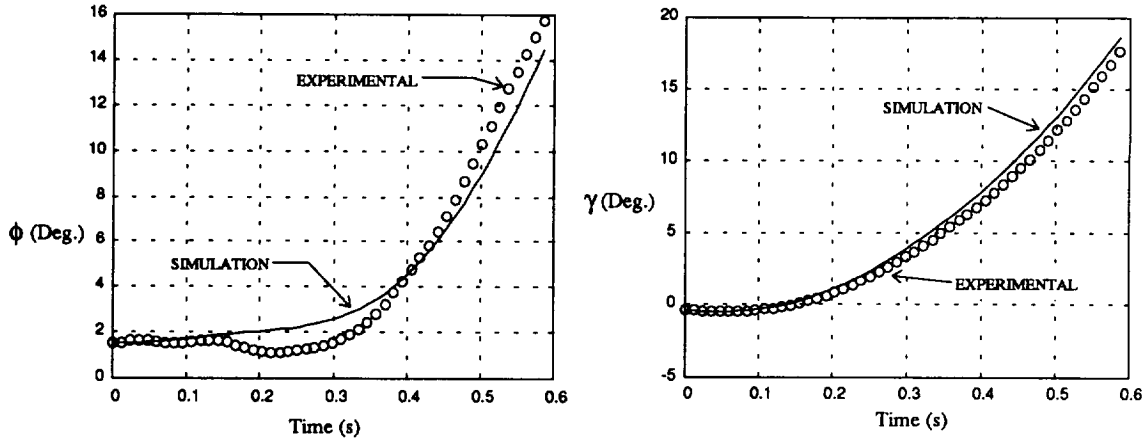

Figure 10: Natural Motion of the Two Degrees of Freedom System. Experiment and Simulation.

Equations of Motion

In order to study the dynamic characteristics of the system it is necessary obtain its equations of motion. For the two degrees of freedom system those are:

$$I_{M_x}\ddot{\phi} + \sin\phi\cos\phi(I_{M_z} - I_{M_y})\dot{\gamma}^2 + \cos\phi I_{M_{xz}}\ddot{\gamma} = M_1$$

$$(I_A + I_{M_y}\sin^2\phi + I_{M_z}\cos^2\phi)\ddot{\gamma} + 2\cos\phi\sin\phi(I_{M_y} - I_{M_z})\dot{\phi}\dot{\gamma} + (\ddot{\phi}\cos\phi - \dot{\phi}^2\sin\phi)I_{M_{xz}} = M_2 \qquad (7)$$

For the current model configuration, where a vertical stabilizer is not present the product of inertia is zero.

M_1 is the moment about the model longitudinal axis,. M_2 is the moment about the γ-axis. M_1 and M_2 are given by:

$$M_1 = M_1^A + M_1^T + M_1^F$$
$$M_2 = M_2^A + M_2^T + M_2^F + M_2^G + M_2^M \qquad (8)$$

Where the superscripts indicates the origin of the moments:

A = aerodynamics
T = air supply tubing
F = friction of bearings and potentiometer
G = gravity restoring moment
M = motor

For $|\phi| < 40°$ the moment caused by to the air supply tubing on the first of equations (8) is negligible[10]. The torque applied by the motor is given by:

$$M_2^M = - M_2^T - M_2^G + I_A \ddot{\gamma} \tag{9}$$

The moments caused by friction of the bearings and potentiometers can be written as:

$$M_1^F = - C_F \dot{\phi} \qquad M_2^F = - D_F \dot{\gamma} \tag{10}$$

C_F and D_F are determined experimentally.

Substituting expressions (9) and (10) in equation (8):

$$\begin{aligned} M_1 &= M_1^A - C_F\dot{\phi} \\ M_2 &= M_2^A - D_F\dot{\gamma} + I_A\ddot{\gamma} \end{aligned} \tag{11}$$

Expressions for the aerodynamic moments M_1^A and M_2^A are necessary to complete the above equations. Wong[3] developed an aerodynamic model for a delta wing undergoing roll oscillations that assumed that the dynamic loads could be approximated by lagged static loads and a pre-specified function of the roll rate. This basic idea is extended by including damping effects proportional to roll and yaw rates, cross-coupling terms in roll and yaw and apparent mass effects due to angular acceleration. The lag in the static loads is justified by comparing static and dynamic flow visualization results which clearly show that the vortex dynamic position lags with respect to the static one[7]. It is known that the strength of the shedding vortices is also affected by the motion of the vehicle. The current approach lumps position and strength effects by lagging the loads to represent their combined effect. Figure 11 shows the structure of the unsteady aerodynamic model in block diagram form. M_1^{AS} and M_2^{AS} represent static roll and yaw moments. The unsteady effects are represented by the time constants τ_1 and τ_2 and functions f_1 and f_2.

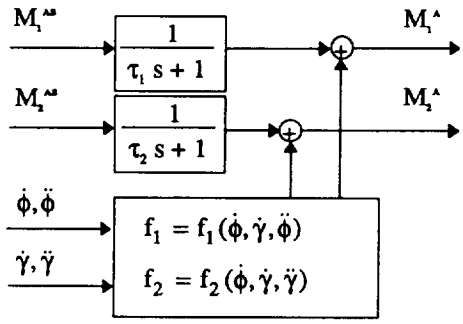

Figure 11: Structure of the Aerodynamic Model. M_1^{AS} and M_2^{AS} represent static roll and yaw moments.

Functions f_1 and f_2 are assumed linear in the angular rates and accelerations:

$$f_1 = C_{\dot{\phi}}\dot{\phi} + C_{\dot{\gamma}}\dot{\gamma} + C_{\ddot{\phi}}\ddot{\phi}$$

$$f_2 = D_{\dot{\phi}}\dot{\phi} + D_{\dot{\gamma}}\dot{\gamma} + D_{\ddot{\gamma}}\ddot{\gamma} \qquad (12)$$

Given the structure shown in Figure 11 and the expressions for f_1 and f_2 , the equations for the aerodynamic moments M_1^A and M_2^A are:

$$M_1^A = \lambda_1 + \zeta_1 + C_{\dot{\phi}}\dot{\phi} + C_{\dot{\gamma}}\dot{\gamma} + C_{\ddot{\phi}}\ddot{\phi}$$

$$M_2^A = \lambda_2 + \zeta_2 + D_{\dot{\phi}}\dot{\phi} + D_{\dot{\gamma}}\dot{\gamma} + D_{\ddot{\gamma}}\ddot{\gamma} \qquad (13)$$

λ_1 and λ_2 are the lagged static roll and yaw moments for C_μ=0, and are given by the following equations:

$$\tau_1\dot{\lambda}_1 + \lambda_1 = M_1^{AS}$$

$$\tau_2\dot{\lambda}_2 + \lambda_2 = M_2^{AS} \qquad (14)$$

ζ_1 and ζ_2 represent the effect of blowing on the roll and yaw moment and are given by:

$$\tau_\phi \dot{\zeta}_1 + \zeta_1 = F_1(C\mu)$$

$$\tau_\gamma \dot{\zeta}_2 + \zeta_2 = F_2(C\mu) \tag{15}$$

Where τ_ϕ and τ_γ are time constants that characterize the roll and yaw moment response to a variation in blowing, ΔC_μ. They include the effect of valve and plenum dynamics as well as the time it takes for the change in the flow structure to affect the moments. Figure 12 shows the response of C_l and C_n for a step input command in C_μ. Also shown are the results of the parameter fitting using equations (15).

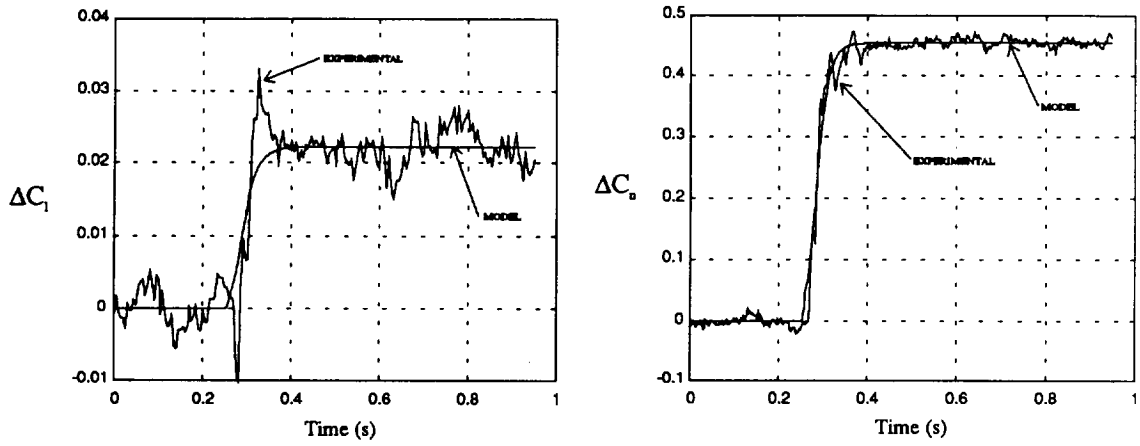

Figure 12: C_l and C_n response to Step Input Command in C_μ. ΔC_l and ΔC_n are used to indicate variation from the initial value.

Substituting equations (11) through (15) into (7) the equations of motion for the two degrees of freedom system are obtained. Dynamic stability derivatives and time constants τ_1 and τ_2 are determined using a minimum least squares fit to the time histories of ϕ and γ for a set of dynamic experiments. Time constants τ_ϕ and τ_γ are determined from the roll and yaw moment response to a step input command in C_μ (Figure 12).

The natural motion of the system is shown in Figure 10. Experimental results are compared with simulation using the aerodynamic model developed. The simulation agrees well with the measured response.

Closed Loop Control

To design a control law that stabilizes the naturally unstable system the equations of motion are linearized as follows: For small static equilibrium roll and yaw angles, i.e. ϕ_E and $\gamma_E << 1$, ϕ and γ are redefined as $\phi-\phi_E$ and $\gamma-\gamma_E$ and equations (7) and (11) are written as:

$$I_{M_x}\ddot{\phi} + C_F\dot{\phi} = M_1^A$$

$$I_{M_z}\ddot{\gamma} + D_F\dot{\gamma} = M_2^A \qquad (16)$$

About the static equilibrium position, M_1^{AS} and M_2^{AS} can be expressed as:

$$M_1^{AS} = C_\phi\phi + C_\gamma\gamma$$

$$M_2^{AS} = D_\phi\phi + D_\gamma\gamma \qquad (17)$$

C_ϕ , C_γ , D_ϕ and D_γ are the static stability derivatives obtained from the curves for the roll and yaw moments versus ϕ and γ.

Equations (15) represent the effect of blowing. For the asymmetric blowing case and $|C_\mu| < 0.01$ F_1 and F_2 are highly non-linear functions of C_μ , as seen in Figure 8. Furthermore operation in this region is prone to generating non-robust control laws because C_1 and C_2 are very sensitive to small variations in blowing. Given the above reasons the low blowing intensities are avoided by employing the following control strategy: A minimum amount of blowing other than zero, C_{μ_0} , is chosen and additional blowing ΔC_μ is added to that value, i.e.:

$$C_\mu \equiv C_{\mu_0} + \Delta C_\mu \qquad (18)$$

The curves for C_1 and C_2 versus ΔC_μ have the general form shown in Figure 13.

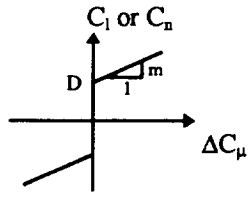

Figure 13: Characteristic of C_l and C_n versus ΔC_μ.

A describing function approach is used to determine the equivalent gain of the curves C_l and C_n versus ΔC_μ. The actual gain, N(A), depends on the amplitude of the input, A, and is given by:

$$N(A) = \frac{4D}{\pi A} + m \tag{19}$$

D and m are defined in Figure 13. An average amplitude is selected for ΔC_μ and used to calculate C_B and D_B the equivalent gains for roll and yaw moment respectively. Expressions for F_1 and F_2 are:

$$F_1 = C_B \Delta C_\mu. \qquad F_2 = D_B \Delta C_\mu. \tag{20}$$

For the symmetric blowing case there is no need to apply the describing function approach because the C_l and C_n variation with ΔC_μ.is fairly linear (Figure 9).

The linearized equations of motion are:

$$(I_{M_x} - C_{\ddot{\phi}})\ddot{\phi} = (C_{\dot{\phi}} - C_F)\dot{\phi} + C_{\dot{\gamma}}\dot{\gamma} + \lambda_1 + \zeta_1$$

$$(I_{M_z} - D_{\dot{\gamma}})\ddot{\gamma} = (D_{\dot{\gamma}} - D_F)\dot{\gamma} + D_{\dot{\phi}}\dot{\phi} + \lambda_2 + \zeta_2$$

$$\tau_1\dot{\lambda}_1 + \lambda_1 = C_\phi\phi + C_\gamma\gamma$$

$$\tau_2\dot{\lambda}_2 + \lambda_2 = D_\phi\phi + D_\gamma\gamma$$

$$\tau_\phi\dot{\zeta}_1 = -\zeta_1 + C_B\Delta C_\mu$$

$$\tau_\gamma\dot{\zeta}_2 = -\zeta_2 + D_B\Delta C_\mu \tag{21}$$

These can be written in the form:

$$\dot{x}(t) = Ax(t) + Bu(t) \tag{22}$$

Where x is the state vector and u the control variable:

$$x(t) \equiv \left[\dot{\phi} \quad \dot{\gamma} \quad \phi \quad \gamma \quad \lambda_1 \quad \lambda_2 \quad \zeta_1 \quad \zeta_2\right]^T$$
$$u(t) \equiv \Delta C_\mu \tag{23}$$

A control logic is designed using the Linear Quadratic Regulator (LQR) method with weights on $\dot{\phi}$, $\dot{\gamma}$, ϕ, γ and ΔC_μ. The result is a gain matrix, -K, that is multiplied by the state vector x(t) to generate the required control, i.e.,

$$u(t) = -Kx(t) \tag{24}$$

This control law requires knowledge of the state vector. ϕ and γ are measured directly. The other state variables are obtained from these measurements and the use of an estimator.

The performance of the closed loop system is shown in Figure 14. The plots show data obtained during a real time closed loop control experiment. In this case the model was released from $\phi \cong 38°$ and $\gamma \cong 14°$. It is seen that the logic makes the system stable and regulates ϕ and γ to close to zero. The third plot shows the control effort, C_μ. Two curves are shown: $C_\mu > 0$ for right side blowing and $C_\mu < 0$ for left side blowing.

Similar results are obtained using symmetric and asymmetric blowing. The disadvantage of the symmetric blowing case is a larger use of air.

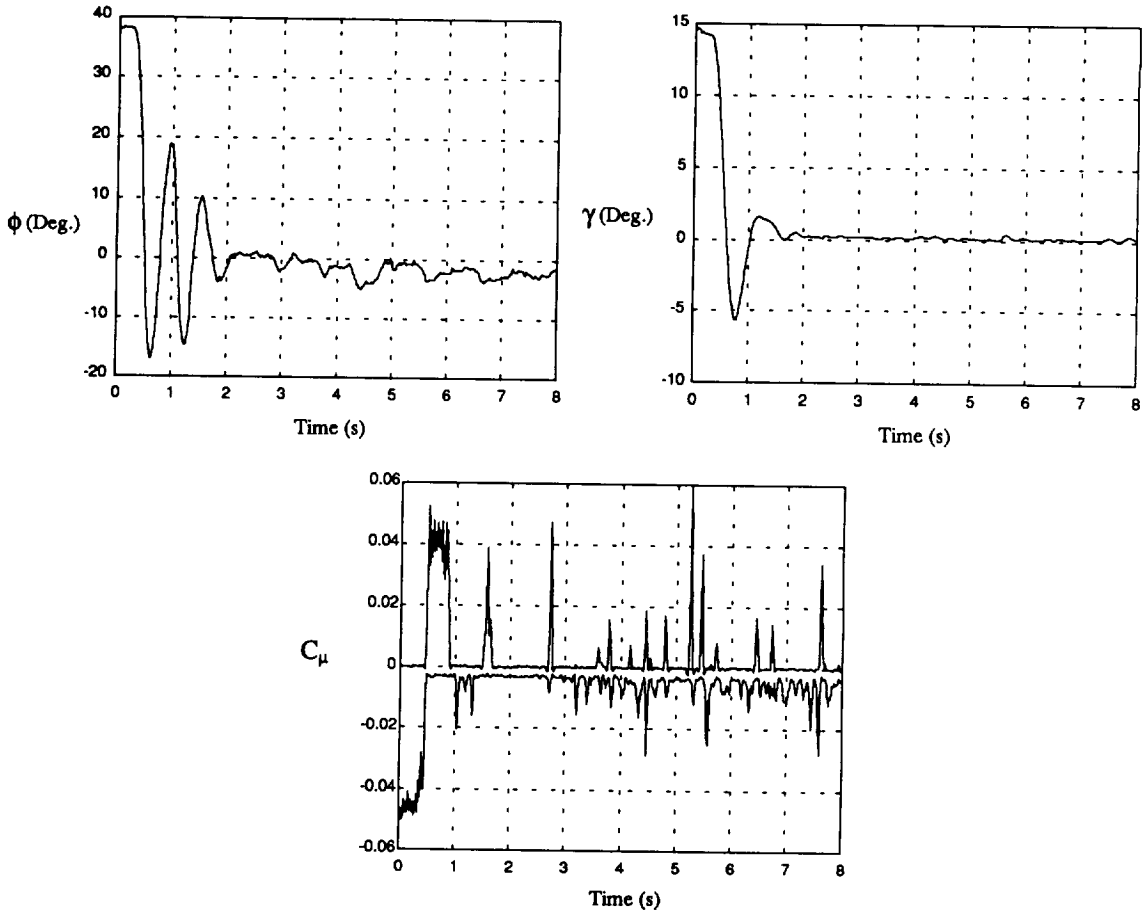

Figure 14: Closed Loop Control of the Two Degrees of Freedom System. Response to Initial Condition. Asymmetric Blowing.

Conclusions

The use forebody tangential blowing (FTB) to stabilize the roll-yaw motion of a delta wing-body model is experimentally demonstrated in the wind tunnel.

An aerodynamic model that is suitable for controls is developed based on: Static measurements of the aerodynamic loads and basic physical representation of the main dynamic effects. The model is validated through dynamic experiments and used in the design of closed loop control laws. The control logic stabilizes the system using blowing as the only actuator. It is shown that asymmetric blowing is a highly non-linear effector that can be linearized by superimposing

symmetric blowing. The transient response of roll and yaw moments to a step input blowing are determined.

Dynamic experiments are conducted using a unique apparatus that allows a wind tunnel model two degrees of freedom, roll and yaw. These experiments show that at 45 degrees angle of attack the natural system is unstable presenting a divergent motion.

The flow structure over the wing-body combination at 45 degrees angle of attack is asymmetric. As determined from flow visualization experiments. The coupling between forebody vortices and wing vortices is strong and an asymmetry that starts on the forebody will determine the structure of the flow downstream. At sections where the wing is present three main vortical structures are discernible. Asymmetric FTB increases the flow asymmetry or inverts it depending on which side of the model blowing is applied. The asymmetry can also be inverted by a change in roll angle. The flow structure is not as sensitive to changes in yaw angle. Differences on the roll and yaw moment dependence on blowing are explained based on the different mechanisms through which they are generated.

Acknowledgments

This work is supported by the NASA-Stanford Joint Institute for Aeronautics and Acoustics, NASA Grant NCC 2-55.

References

1. Ericsson, L.E. and Reding, J.P., "Alleviation of Vortex Induced Asymmetric Loads", Journal of Spacecraft and Rockets, Vol 17, Nov.-Dec. 1980, pp. 546-553.

2. Rao, D. M., Moskovitz, C., and Murri, D. G., "Forebody Vortex Management for Yaw Control at High Angles of Attack," Journal of Aircraft, Vol. 24, No. 4, p. 248-254, April 1987.

3. Wong, G.S., "Experiments in the Control of Wing Rock at High Angles of Attack Using Tangential Leading Edge Blowing," Ph.D. Dissertation, Aeronautics Department, Stanford University, 1991.

4. Ng, T. T., and Malcolm, G. N., "Aerodynamic Control Using Forebody Strakes," AIAA Paper 91-0618.

5. Celik, Z.Z. and Roberts, L., "Vortical Flow Control on a Wing-Body Combination Using Tangential Blowing," AIAA Paper 92-4430.

6. Celik, Z.Z., Roberts, L. and Pedreiro, N., "The Control of Wing Rock by Forebody Blowing," AIAA Paper 93-3685.

7. Celik, Z.Z., Roberts, L. and Pedreiro, N., "Dynamic Roll and Yaw Control by Tangential Forebody Blowing," AIAA Paper 94-1853.

8. Adams, R. J., Buffington, J. M., and Banda, S. S., "Active Vortex Flow Control for VISTA F-16 Envelope Expansion," AIAA Paper 94-3681.

9. Degani, D., "Numerical Investigation of the Origin of Vortex Asymmetry," AIAA Paper 90-0593.

10. Pedreiro, N., "Experiments in Aircraft Roll-Yaw Control Using Forebody Tangential Blowing," Ph.D. Dissertation (to be published), Aeronautics and Astronautics Department, Stanford University.